Journal Pre-proofs

Improving fatigue resistance of railway axles by cold rolling: process optimisation and new experimental evidences

D. Regazzi, S. Cantini, S. Cervello, A. Lo Conte, S. Foletti, A. Pourheidar, S. Beretta

PII: S0142-1123(20)30134-1
DOI: https://doi.org/10.1016/j.ijfatigue.2020.105603
Reference: JIJF 105603

To appear in: *International Journal of Fatigue*

Received Date: 5 October 2019
Revised Date: 27 February 2020
Accepted Date: 16 March 2020

Please cite this article as: Regazzi, D., Cantini, S., Cervello, S., Conte, A.L., Foletti, S., Pourheidar, A., Beretta, S., Improving fatigue resistance of railway axles by cold rolling: process optimisation and new experimental evidences, *International Journal of Fatigue* (2020), doi: https://doi.org/10.1016/j.ijfatigue.2020.105603

Improving fatigue resistance of railway axles by cold rolling: process optimisation and new experimental evidences

D. Regazzi[a], S. Cantini[a], S. Cervello[a], A. Lo Conte[b], S. Foletti[b], A. Pourheidar[b], S. Beretta*

[a] *LucchiniRS, Via G. Paglia 2, Lovere (BG)*
[b] *Politecnico di Milano, Dipartimento di Meccanica, Via La Masa 1, 20156 Milano (IT)*

Abstract

Cold rolling is a relatively simple process known as a method to increase the surface hardness and the mechanical fatigue resistance of metal components by the introduction of residual compressive stresses. Cold rolling is also particularly convenient as it is applied in the final part of the manufacturing process. Despite the process being quite common in the manufacturing of various mechanical components, very limited information is available about the actual advantages that are achievable on safety critical components like railway axles. This paper focuses on both optimisation of the process parameters adopted on the Lucchini RS and on the advantages that are obtained when a well calibrated process is applied. The process is optimized by an analytical model, validated by means of an extensive number of residual stress measurements using the X-Ray Diffraction method, that estimates the residual stress profile that is generated under the surface depending on different parameters (force, roller geometry, roller feed, axle geometry and steel grade). An overview of various advantages, demonstrated by an extended series of experimental full-scale tests, is then shown: an increase in the fatigue limit even in the presence of artificial micro-notches and corrosion fatigue. An analysis of the driving force at the crack tip is able to confirm the experimental evidences.

Keywords: railway axles, fatigue, cold rolling, crack propagation, corrosion-fatigue

*Corresponding author
Email address: stefano.beretta@polimi.it (S. Beretta)

1. INTRODUCTION

The fatigue life and life propagation of railway axles can be greatly improved by the induction of compressive residual stresses, the primary source of which can be suitable heat treatment [1, 2, 3]. Alternatively, cold rolling is a very effective manufacturing technology to build up compressive residual stresses in the surface layer of the wheelset axles in a controlled and repeatable way [4, 5]. The technological parameters of cold rolling are determined by the "tool/workpiece" interaction, where the most important are the geometry of the cold rolling device, the geometry of the wheelset axle, the cold rolling force, the feeding of the tool and the material properties of tool and axle. The following project specific requirements play a significant role in the specification of the above cold rolling parameters: machining reserve of each axle segment (e.g. shaft, seat) and the crack size detectable by Ultrasonic Testing (UT) inspection. In order to extend the lifetime of the railway axle, it is desirable that, after the technological process, the depth at which residual compressive stress occurs is both deeper than the machining reserve, allowing for re-machining in service thus maintaining the compressive state, and deeper than the detectable crack size, for closing the edges of a possible crack in service by the compressive stresses. The importance of cold rolling is due to the increased fatigue stress and crack inhibition effect coming from the residual compressive stress in the surface and sub-surface layer[2, 6]. With these effects the service life of the axles can be increased, and the maintenance costs can be reduced due to an increased distance between ultrasonic inspection intervals resulting from a higher crack propagation threshold and a lower growth rate.

In this paper we explain new concepts for simulating the residual stress

profile and validating it, together with a new series of experiments that significantly extend the results previously obtained at PoliMI [6]. In detail, new experiments on EA4T steel show a significant improvement of fatigue strength in full-scale axles, a further validation of previous tests on axles containing defects, a new set of experiments on full-scale specimens exposed to corrosion-fatigue. Evidence from the latter evidences clearly shows the ability of cold-rolling to inhibit the propagation and transition from environmental-assisted cracks to long cracks sustained in conventional crack growth mechanisms.

2. Analytical model and its validation

The analytical model for the prediction of the residual stresses induced by cold rolling is based on the original model proposed by Guechichi et al. [7] for predicting the residual stresses due to shot-peening. The model assumes a periodic time dependent stress field as a linear combination of the elastic stress field and the residual stress field:

$$\sigma = \sigma^{el} + \sigma^{r} \tag{1}$$

where bold denotes a tensor quantity. The elastic stress field σ^{el} has been computed using the equation proposed by Sackfield and Hills [8]. The contact area dimensions are related to the roller radii, the applied contact force and the shape of the cold rolled part. The approximate analytical model of Hertzian theory proposed by Antoine et al. [9] was applied to calculate the dimension a, b of the elliptical area of contact and the Hertzian contact pressure.

The total strain produced by the roller during a single rolling step can

be written in terms of an inelastic and an elastic part:

$$\epsilon = \epsilon^{el} + \epsilon^{ine} == \epsilon^{el} + \epsilon^{p} + M\sigma^{r} \tag{2}$$

where the inelastic portion is a superposition of the irreversible plastic strain and the strain resulting from the residual stresses. The strains corresponding to the residual stresses are governed by the law of elasticity by considering the elastic compliance matrix M. The irreversible plastic strain is obtained in the framework of a cyclic plasticity model with the normality flow rule:

$$d\epsilon^{p} = dp.n \tag{3}$$

where n is the unit exterior normal to the yield surface for a given deviatoric stress state and dp is the equivalent plastic strain increment. By forcing the inelastic strains during each passage of the load to be zero, Eqs. 2 and 3 can be solved for obtaining the residual stress increment with respect to the equivalent plastic strain increment:

$$\begin{cases} \frac{d\sigma_x^r}{dp} = -\frac{E}{1-\nu^2}(n_x + n_y\nu) \\ \frac{d\sigma_y^r}{dp} = -\frac{E}{1-\nu^2}(n_y + n_x\nu) \end{cases} \tag{4}$$

where the residual stress field is approximated by considering the vertical residual stress to be small if compared to the longitudinal and circumferential residual stress leading to the condition $\sigma_z^r = 0$. More details about the analytical model and its implementation can be found in [10].

In order to validate the analytical model, a dedicated experimental campaign was started. Four axles made of EA4T [11] and coming from standard production were cold-rolled, mixing up the most interesting parameters in

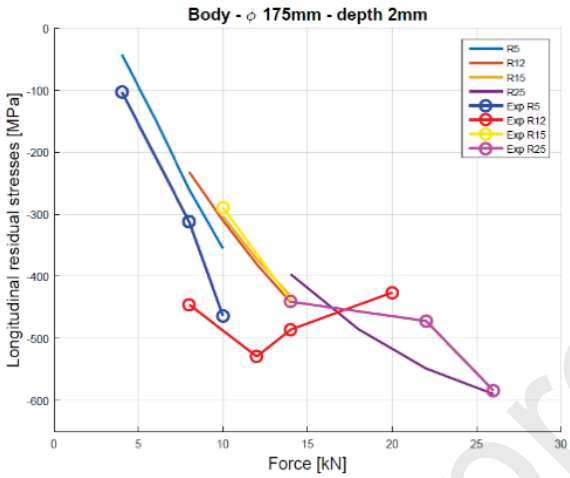

Figure 1: Comparison between calculations and experimental residual stress measurements, due to cold-rolling, at 2 mm depth.

order to validate the analytical model in all the cold rolling conditions. Four values were chosen for each of the three parameters of roller radius, axle diameter and applied force, leading to 64 combinations in total, all compared to the same one by calculation. Each of the 64 combinations was investigated by X-ray Diffraction (XRD) diffractometer, at increasing steps in depth, up to 2.5 mm. An example of the comparison is shown in Figure 1, considering the experimental scatter due to the position, real depth, number of experimental measurements a good agreement can be seen between the numerical and experimental results, It is worth to note that the predictions are always conservative with respect to the experimental results. Once developed and validated, the analytical model was transposed into a dedicated calculation software, in order to be able to predict the residual stress field for each cold-rolled project in production. Moreover, the analytical model is also used in order to optimize the technological parameters, given the requirements of each geometry and material.

In order to verify the persistence of the residual compressive stresses after in-service maintenance, as part of a German research program [12] the changing of the under-layer residual stress was examined in the case of machining of the cold rolled axle surface. It was demonstrated that, under service conditions there was no significant stress relaxation.

The transition point between the compressive and the tensile stresses was approximately at 9 mm below the new axle surface. The volume or respective surfaces of the cross sections with the compressive stress and the tensile stress must be in equilibrium in any cross section of the axle. The modeling showed that if some surface layers within the compressive stress zone are removed, the transition point between the compressive and tensile stress basically does not change, remaining approximately at the depth of 9 mm. To maintain the stress equilibrium in the cross section between the stress directions, the amplitude of the compressive residual stress has to increase. In the simulation the machining reserve is $2,5$. The compressive residual stress after cold rolling is approximately $350MPa$ at the depth of $2,5$. It is worth noting that after machining of the axle the new residual surface stress will be increased approximately from $350MPa$ (the value at2.5 depth) to $430MPa$ (the value on the new surface after removal of $2,5$ of the reserve material). In the simulation it was supposed that the machining itself does not cause any additional residual stress due to the effect of cold rolling.

3. Experimental evidence

In order to better understand the increase in the mechanical properties of the full-scale axles after cold-rolling, several experimental campaigns

were started during recent years, in order to quantify the benefit from the product's point of view, in terms of fatigue and crack initiation resistance.

3.1. Full-scale fatigue tests

Full-scale tests for to verify the increase in the $F1$ fatigue resistance of cold-rolled axles compared to plain axles was performed, adopting 10 specially designed full-scale specimens (See Fig 3.a) tested at Lucchini RS laboratories under resonant test benches, shown in Figure 3.b . The axles are made of EA4T steel according to EN 13261, quenched and tempered 25CrMo4, with the tensile properties and chemical composition according to Tab 1 and Tab 2 respectively. As it is illustrated in Fig 2 a thin layer of micro-structural distortion (in the order of $8-10\ \mu m$) is generated in the surface due to the plastic deformations imposed by the cold-rolling process in which the hardness in the cold-rolled surfaces is about 270-300 HV.

Table 1: Tensile properties of the EA4T steel.

Grade	Tensile Strength			Elongation	
EA4T	R_{eh}(N/mm^2)	R_m (N/mm^2)	A_5 %	KU longitudinal (J) at 20^{o}C	KU transverse (J) at 20^{o}C
	≥ 420	$\geq 650-800$	≥ 18	≥ 40	≥ 25

Table 2: The Chemical composition of the EA4T steel

Grade	C	Si	Mn	P[a]	S	Cr	Cu	Mo	Ni	V
EA4T	0.22	0.15	0.50			0.90		0.15		
	0.29	0.40	0.80	0.020	0.015[b]	1.20	0.30	0.30	0.30	0.06

[a] A maximum content of 0.025% may be agreed at the time of inquiry and the order

[b] A minimum sulfur content may be agreed at the time of inquiry and the order according to the steel making process, in order to safeguard against the hydrogen embrittlement

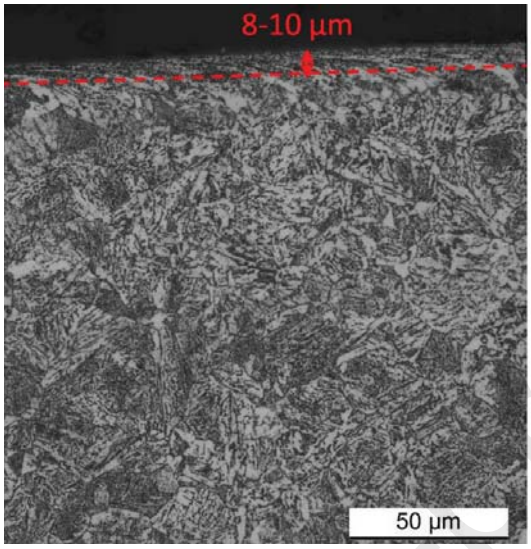

Figure 2: Thin layer of micro-structure distortion imposed by the cold-rolling process.

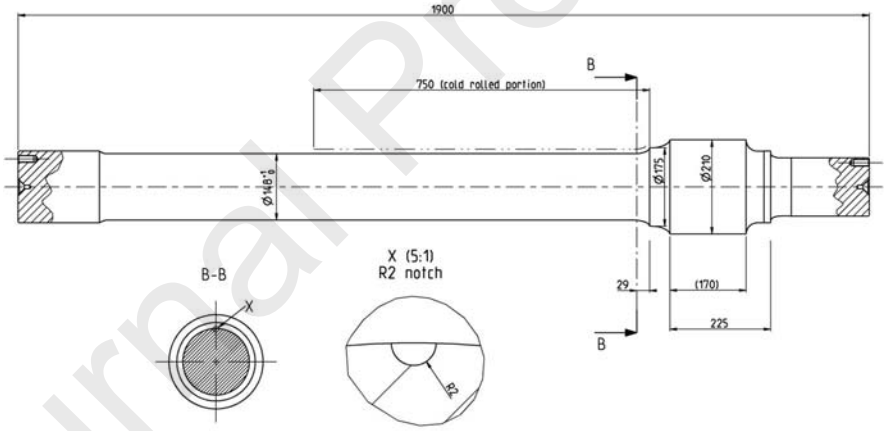

(a)

(b)

Figure 3: Testing setup of cold-rolled axles: a) The adopted full scale specimen for corrosion fatigue test with EDM semicircular micronotches with depth of 2 mm; b) resonant test bench.

A staircase test was performed, starting from $320MPa$ stress amplitude, at stress ratio -1 in the transition close to the seat, and increasing in $20MPa$ increments up to failure. The results of the staircase sequence are represented in Figure 4. As can be seen from the picture, the application of cold-rolling to EA4T axles is able to increase the fatigue resistance of the axle body by more than 25%, increasing the 50% fatigue limit from about $310MPa$, as evaluated in the context of the European Euraxles project [13], up to about $390MPa$.

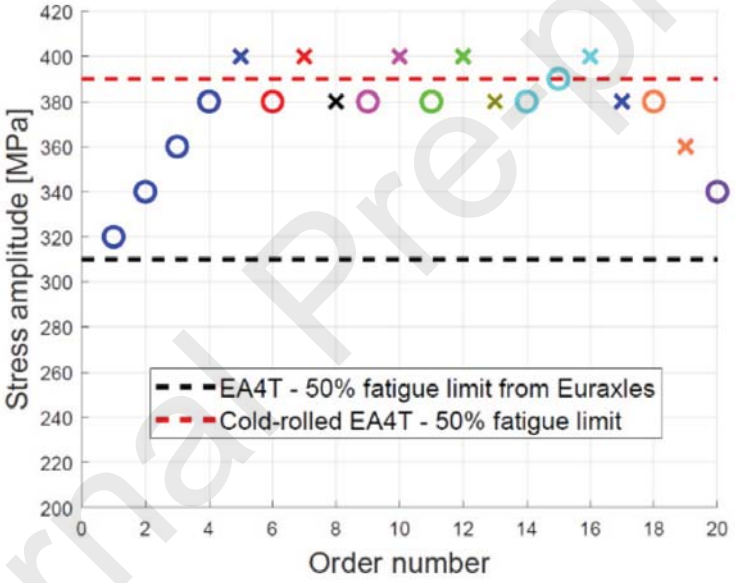

Figure 4: Staircase of full scale cold-rolled axles made of EA4T in order to determine the fatigue limit of a smooth axle.

There is the possibility of adopting the higher fatigue limit of the cold-rolled axles in order to reduce the mass of the wheelset. So a new fatigue test campaign, that is consistent with the procedure in Annex D of the standard $EN13103-1$ [14], was carried out. In order to quantify the increase of the safety factor, the new experimental campaign was started, introducing

artificial Electrical Discharge Machining (EDM) micro-notches in the most stressed transition of the same axle design already adopted for fatigue. Semi-circular artificial notches of 2 mm radius were introduced, and the staircase test was repeated. The results are shown in Figure 5.

•. As can be seen from the plotted data, a fatigue limit higher than $300MPa$ is possible even in presence of defects. From another point of view, even in presence of 2 mm initial defect, all the cold-rolled axles are able to survive a full-scale qualification test of 10 million cycles at $240MPa$, as prescribed by $EN13261$ standard [11] to simulate an infinite lifetime for the component.

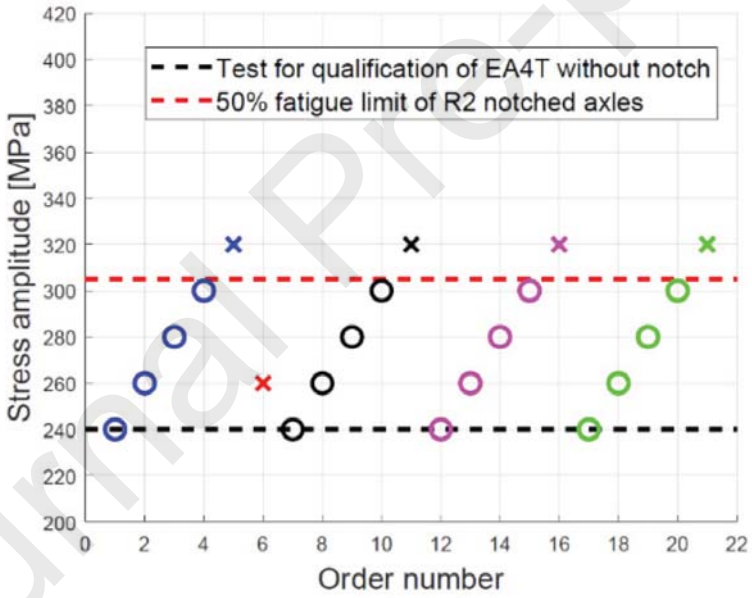

Figure 5: Short staircase of full-scale axles made of EA4T, in order to obtain the fatigue limit in presence of the artificial notches ($a = 2\,[mm]$ machined by EDM in the T-transition close to the wheel seat.

3.2. Crack propagation test

Crack propagation tests are the practical evaluation methods for determining Nondestructive testing (NDT) inspection intervals for wheelset axles. Actually, the railway industry is quite unique from the point of view of periodical NDT inspections, wheelsets-axles being inspected on a regularly basis both during service and during overhauling, in order to promptly detect surface defects resulting from service. The UT method, with its different techniques (see for instance [15]), is fairly widespread for the inspection of such critical safety components. Crack propagation tests like any other tests must fulfil the basic requirements of accuracy, reproducibility and representativeness: in particular the conformity of the test piece with the standard product and the load on the test bench with the service load play a key role. Several crack propagation tests were carried out in the past, see for instance [16, 6]. Similar set of experiments was carried out by Siemens Mobility, as well as Lucchini RS [12] on cold rolled axles in presence of micro-notches with the depth of $4\,[mm]$, under service stress spectra. It was found that the cracks were not able to propagate. Considering that a crack with $a = 4\,[mm]$ is much larger than defects induced surface damages [17], it is clear that cold rolling has a great potential for reducing the periodicity of ultrasonic inspections and the related inspection costs.

4. Corrosion fatigue tests

As it is summarized in Tab 4, two corrosion-fatigue tests were carried out on rolled axles in which, after cold rolling, two EMD semi-circular notches with a depth $a = 1$ mm were machined. The tests were carried out at $\Delta\sigma = 320$ and $\Delta\sigma = 240$ using a 3 point bending bench . Figure 6 shows

an overview of the adopted full-scale specimen and test bench used at Politecnico di Milano (PoliMi) [18].

Corrosion conditions were continuously applied to specimens by means of a dedicated dropping system with reservoir and a small pump ensuring a dripping flow rate of $80cc/min$. The artificial rainwater solution, characterized by $pH = 6$, was replaced every day. Other test details in [18].

Tests were subjected to programmed stops in order to measure the distribution of propagating cracks using the optical device [19], that was set up for the WOLAXIM project.

Crack length population measurements were obtained after several applications of deox gel onto the axle surface in order to remove surface rust,(See figure 8). Three different 10 mm^2 areas were inspected for each axle comparing the results with those obtained for axles without cold rolling (Axle 056). After cleaning procedure was completed, the surface observed by the optical microscope (see [19]). Table 4 summarized the number of cycles related to cracks population measurements.

Table 3: Detail of the full-scale corrosion fatigue tests

Axle name	Surface treatment	Defect radius (mm)	Applied stress (MPa)	Results
A056	Q & T	ho defect	320	Run out at $3.6 \cdot 10^6$
A057	Cold rolled	1	320	Run out at $1 \cdot 10^7$
A058	Cold rolled	1	240	Run out at $3 \cdot 10^7$

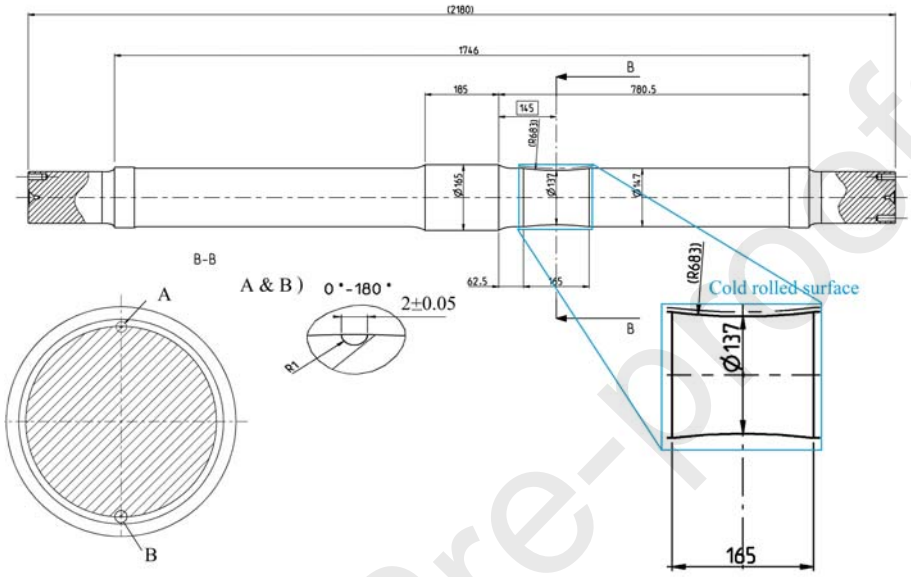

(a)

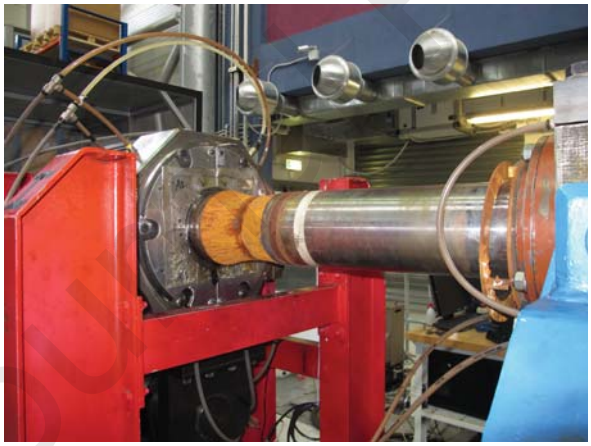

(b)

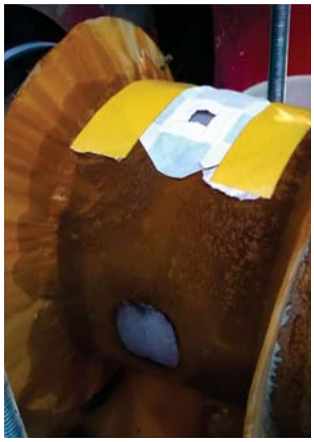

(c)

Figure 6: Details of the corrosion fatigue experiments: a) The adopted full scale specimen with EDM notches; b) test bench with the dropping system; c) detailed observations on 10 mm^2 areas.

Table 4: Test stops for cracks population detection [cycles]

Axle code	A056	A057	A058
Stress range	$\Delta S = 320$ MPa	$\Delta S = 320$ MPa	$\Delta S = 240$ MPa
stop #1	1 000 000	1 000 000	1 000 000
stop #2	2 293 000	2 293 000	2 000 000
stop #3	3 227 048	3 227 048	3 000 000
stop #4	–	4 317 000	4 000 000
stop #5	–	6 000 000	6 000 000
stop #6	–	8 000 000	8 000 000
stop #7	–	10 000 000	10 000 000
stop #8	–	–	20 000 000
stop #9	–	–	30 000 000

4.1. Results and corrosion-fatigue damage

The first important result that was obtained from the microscope observations is that the early development of corrosion-fatigue cracks is slightly reduced because of the beneficial effect of cold-rolling (Figure 7). However, even if the crack density is lower in cold-rolled axles, from $3.2 \cdot 10^6$ cycles the two distributions appear identical.

Similar results were also obtained on the axle 058 tested at $\Delta S = 240\,[MPa]$: the distribution of cracks was similar to the one measured in [20] from $6 \cdot 10^6$ cycles.

The most important result came from the observations of the micronotches is that the two axles (respectively tested at $\Delta\sigma = 320\ MPa$ and $240 MPa$) survived the corrosion fatigue tests at $1 \cdot 10^7$ and $3 \cdot 10^7$ cycles without observing any significant crack propagation out of the two micro notches. This is a very important outcome showing that cold-rolled axles survived under corrosion-fatigue beyond the life of non-rolled axles previously tested [20].

In order to better investigate the possible development of cracks the surface of the hourglass shaped axle was machined in order to obtain an hollow section. This section was then cut into several slices with a width $w = 20$ [mm] for subsequent observations under SEM. The schematics of the cuts for the slices is shown in Fig. 9.

The slices containing the two mico notches were broken under liquid nitrogen for the axle tested at $\Delta S = 320 MPa$. The observation under SEM (see Fig. 10) revealed only a tiny development of a 200 μm crack ahead of the micronotch. The corrosion-fatigue cracks, at static failure, revealed a layer with an average depth of 400 μm.

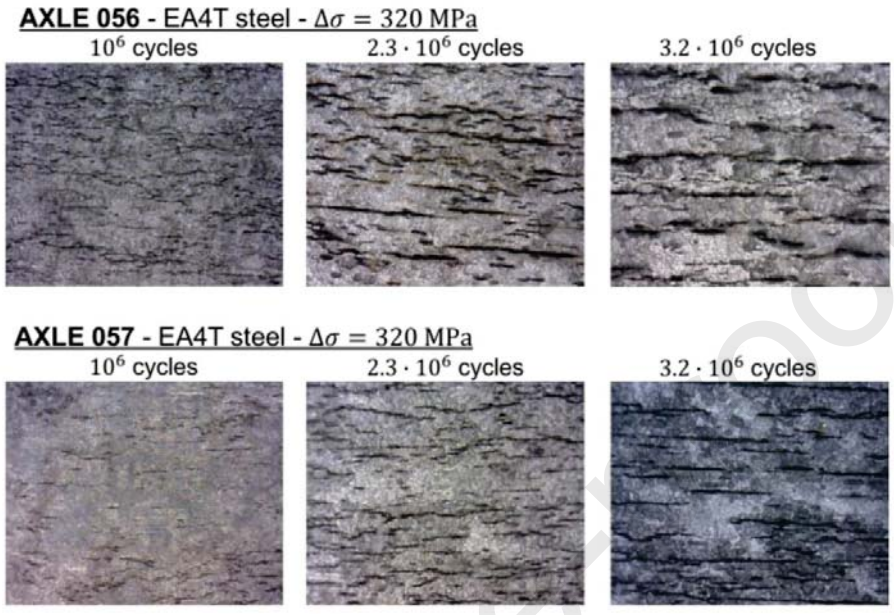

(a)

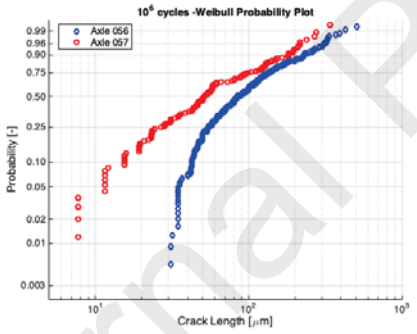

(b)

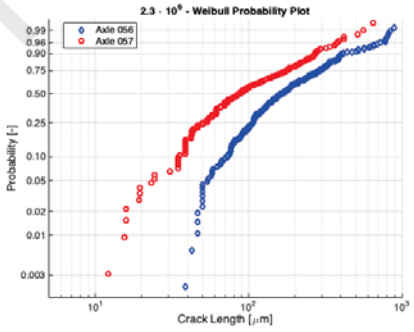

(c)

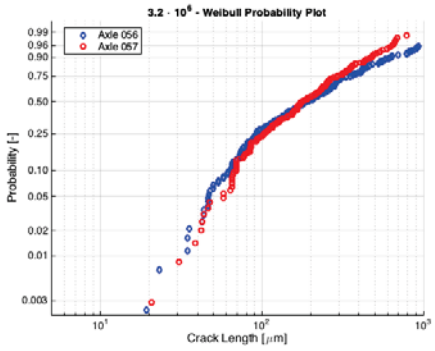

(d)

Figure 7: Experimental results - Comparative observations of axle surface exposed to corrosion-fatigue: a) Axle 056 (standard surface) versus Axle 057 (cold rolled surface); b) distributions of the corrosion-fatigue surface cracks at $N = 10^6$; c) distributions of the corrosion-fatigue surface cracks at $N = 2.3 \cdot 10^6$; d) distributions of the corrosion-fatigue surface cracks at $N = 3.2 \cdot 10^6$

The slices of the axle tested at $\Delta S = 320 MPa$ were examined under SEM and cut in the longitudinal direction in order to observe the development of cracks at the bottom of the defects. The observation revealed the presence of non-propagating cracks and confirmed a depth of 200 μm for the corrosion cracks ahead of the micronotch.

(a)

(b)

(c)

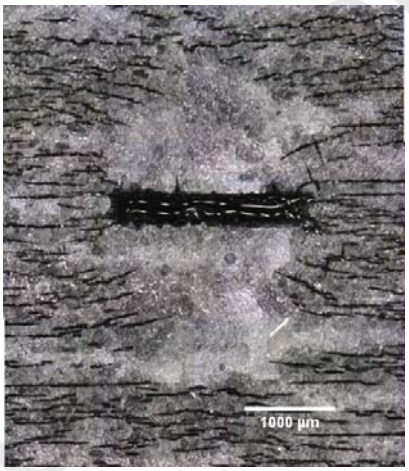

(d)

(e)

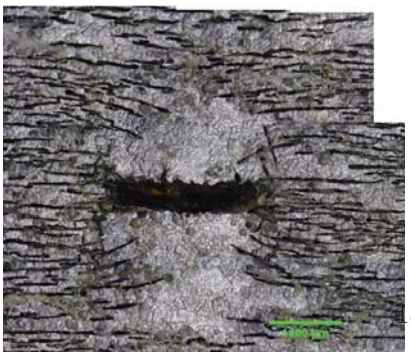

(f)

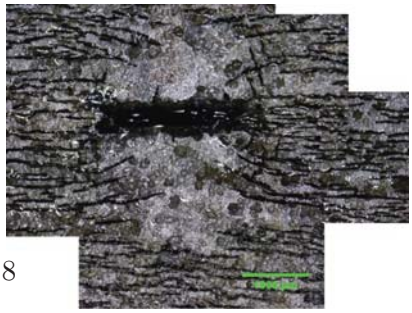

(g)

Figure 8: Full-scale tests artificial defect (axle 057, $\Delta S = 320\,[MPa]$)- Defect A: (a) 1 000 000 cycles (b) 2 293 000 cycles (c) 3 227 048 cycles (d) 4 317 000 cycles (e) 6 000 000 cycles (f) 8 000 000 cycles (g) 10 000 000 cycles

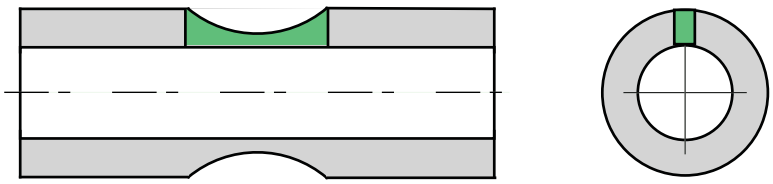

Figure 9: Scheme of the cutout of the slices for observing the development of surface corrosion-fatigue cracks

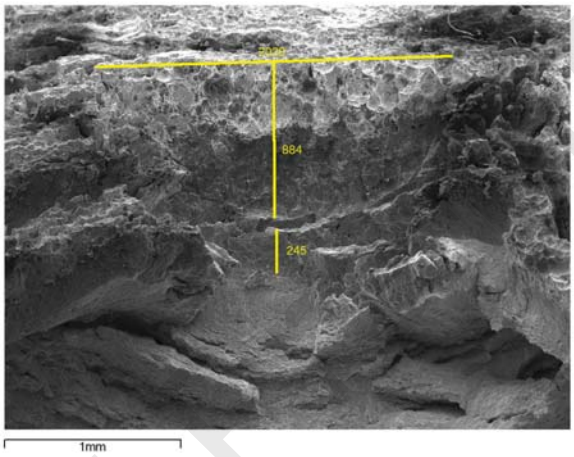

(a)

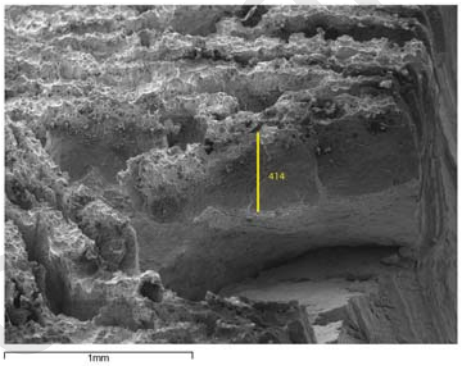

(b)

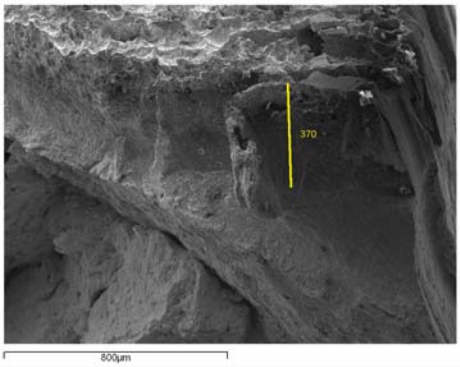

(c)

Figure 10: Axle A057 - Observations of defect B after static failure ($N = 10^7$ cycles at $\Delta S = 320\,[MPa]$, measurements of details expressed in $[\mu m]$)

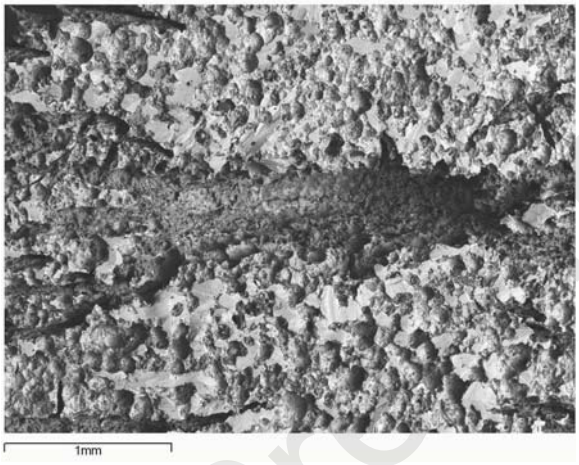

(a)

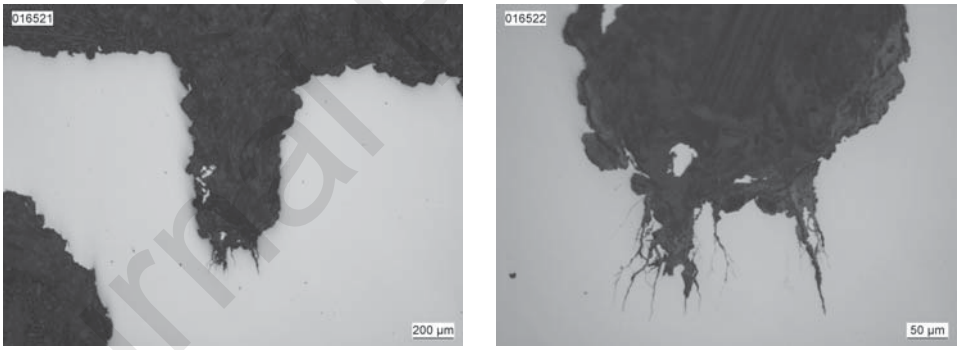

(b) (c)

Figure 11: Axle A058 - Observations of defect B after static failure ($N = 3 \cdot 10^7$ cycles at $\Delta S = 240\,[MPa]$): a) surface view; b-c) polished cross sections of the artificial micro notches

5. Discussion and interpretation of results

5.1. Fatigue tests in air

As for the increase in fatigue strength of smooth cold-rolled axles, this result is perfectly in accordance with the wide range of literature about the subject and the available results [4, 5].

The analysis was therefore concentrated on understanding the enhanced fatigue properties in presence of the artificial micro notches. The effect of local increase of properties [21] for the rolled surface layer were not taken into account, because we examined the prospective crack propagation from the micro-notches (no significant microstructural changes at depths ¿ 10 μm).

The analyses was carried out by treating the micro notches as cracks, then the SIF was calculated with the Weight Function (WF) [22] (see section 5.2) under the stresses due to the bending moments M_b and the stresses due to the residual stress profile were estimated using the analytical model described in Sect. 2 as:

$$K_{max} = K_{res} + 0.5 \cdot \Delta K \tag{5}$$

where K_{res} is the SIF due to residual stresses and ΔK is the stress intensity factor range due to bending moment M_b. The scheme for the calculation is shown in Fig 12.b together with the residual stress profile.

In detail, for the tests at $\Delta S = 320\,[MPa]$ the residual stress profile calculated in Sect. 2 was updated considering the relaxation of the residual stresses for the attainment of a condition of elastic shakedown under the cyclic stress [23, 24, 25]. The results of the SIF for the fatigue limit tests on micronotched axles are reported in Tab. 5.

Table 5: The SIF analysis of full-scale axle fatigue tests in air

test type	crack $[\mu m]$	K_{res} $[MPa\sqrt{m}]$	ΔK $[MPa\sqrt{m}]$	K_{max} $[MPa\sqrt{m}]$
fatigue test $S_{max} = 320\,[MPa]$	(2000 : 2000)	-10.22	32.38	5.96

As it can be seen at point A $K_{max} > 0\,[MPa\sqrt{m}]$ for the axles failed in the transition at $\Delta S = 320\,[MPa]$. This value corresponds to threshold K_{max} for $R = -4.4$ for EA4T reported in [26] and so it provides support to the experimental evidence of the fatigue limit in presence of micronotches.

This result is completely opposite to what we have so far observed for tests under variable amplitude loading, where no growth is observed from the micronotches [6, 12]. These tests are characterized by a maximum SIF (at the maximum stress level applied during the block loading) $K_{max} < 0$. Therefore, the absence of crack development can be justified because micro-cracks can propagate only if tensile part of the loading cycle for which for which $\Delta K^{+} > \Delta K_{eff}$ [27, 28, 29, 30, 31] .

Table 6: Statistics of rainy days for European cities

city	*rainy days per year*	*ratio*
Bruxelles	228	1 : 1.6
London	164	1 : 2.2
Paris	171	1 : 2.1
Berlin	180	1 : 2
Budapest	156	1 : 2.3
Milan	144	1 : 2.5
Madrid	96	1 : 3.8

5.2. Corrosion-fatigue tests

In first instance, the conclusion that we can draw from the two tests is that the two axles survived the corrosion-fatigue conditions that had led to failures of full-scale axles tested in previous projects.

This looks to be especially important for axle $A058$ that did not show any development of cracks for a number of cycles $N = 30 \cdot 10^6$ cycles that correspond to a mileage of $90,000$ kilometres under rainwater.

Considering the available weather statistics for most European cities, shown in Tab. 6, it can be concluded that a conservative ratio $1:2$ corresponds to the fraction of rainy days during a year. It was observed in [32] that only the fatigue cycles exposed to corrosion are relevant for corrosion-fatigue because in those cycles microcrack can propagate at $\Delta K < \Delta K_{th}$ because of the corrosion. Therefore, considering the 1: 2 ratio for rainy days, it can be said that the mileage for axle $A058$ should correspond to at least $180,000$ kilometres of service, which is certainly a significant safe service in presence of corrosion-fatigue.

Also for the axles subjected to corrosion fatigue the driving force ahead of the micronotches/ cracks was calculated with the following hypotheses:

- the SIF at the tip of a prospective crack is calculated as:

$$K = \int_0^a \sigma_z \cdot w(x,a)dx \tag{6}$$

  where x is a coordinate along the crack depth (radial coordinate for the rotating axle) and $w(x,a)$ is the weight function by Wang & Lambert [22] for semi-elliptical cracks on plates (axle diameter is taken for width and thickness of the plate);

- The bending stress is assumed to be undisturbed by the presence of corrosion cracks (this corresponds to imagining that: i- the deformation of the axle section is not influenced by the thinning due to corrosion; ii - there is no shielding due to the corrosion-cracks).

The results for some significant cracks (shown in the figures) are shown in Tab. 7, where for the corrosion-fatigue surface cracks (fig. 10b) we took $c = 10 \cdot a$ to represent a shallow surface crack. The important conclusion that

Table 7: Calculation of the driving force for some cracks

ref.	*crack size (a:c)* $[\mu m]$	K_{res} $[MPa\sqrt{m}]$	ΔK $[MPa\sqrt{m}]$	K_{max} $[MPa\sqrt{m}]$
Fig. 10.a	(1130 : 1130)	-23.60	12.26	-17.45
Fig. 10.b	(420 : 4200)	-22.18	12.66	-15.84
Fig. 11.a + 11.c	(1200 : 1200)	-24.21	9.46	-19.48

can be drawn is that ahead of the corrosion- fatigue cracks $K_{max} < 0$. Since in the models for corrosion-fatigue damage [20, 33] the failure is triggered by the transition from corrosion-fatigue to fatigue when $\Delta K > \Delta K_{th,LC}$, it is clear that the inability of the cracks to propagate in Mode I prevents the onset of the final fatigue failure.

This important conclusion is supported by the observations: the cold-rolling does not prevent the formation of corrosion-fatigue cracks, but those cracks are not able to switch to Mode I propagation and the phenomenon is self-limiting. Moreover, the evidence of this self-limitation even in presence of micro-notches suggests that, even in the odd combination of corrosion-fatigue with surface dents due to impacts [17, 34], the concept $K_{max} < 0 \rightarrow$ no fatigue failure can be applied also in the presence of corrosion-fatigue.

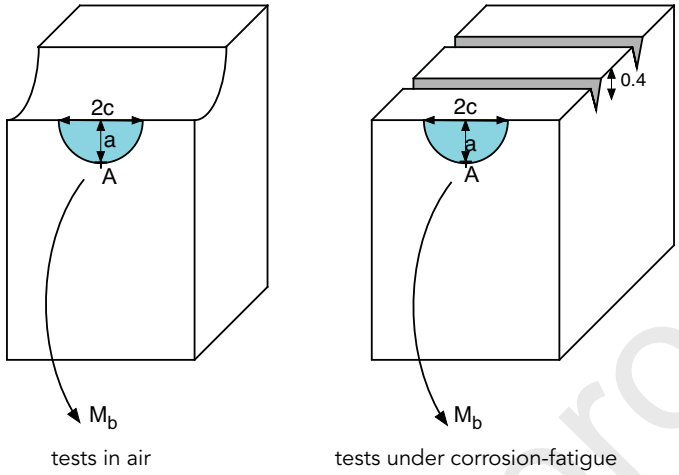

(a)

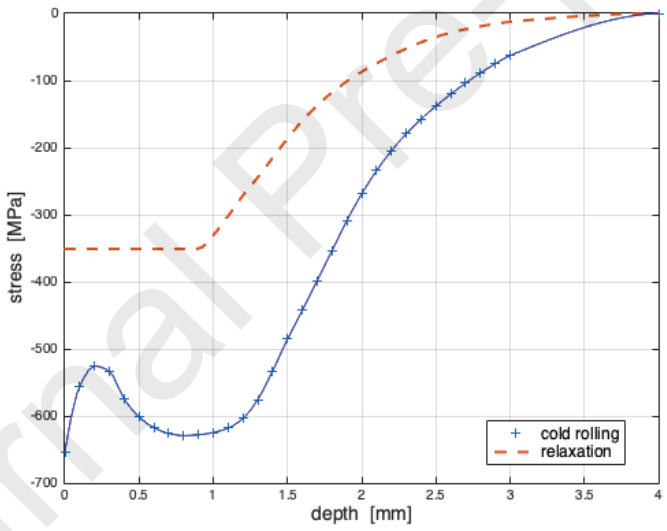

(b)

Figure 12: Calculation of the driving force for cracks: a) scheme of the analysis reference geometry for calculation of SIF at point A; b) residual stress profiles considered.

6. Conclusions

In this paper we have presented some important evidence about the effects of cold-rolling on fatigue of axles made of EA4T and tested in full

scale. The results can be summarized as follows:

- the full scale fatigue resistance of EA4T axle body increases by 25%;
- cold-rolled axles with micro notches with a depth of 2 mm have a fatigue strength comparable to fatigue strength of smooth (no defect) EA4T axles.
- cold-rolled axles have a longer life that usual EA4T axles exposed to corrosion-fatigue;
- the residual stresses prevent the transition to Mode I propagation of the naturally developed corrosion-fatigue cracks and their depth was found to be limited to a surface layer of $\approx 400\,\mu m$.

Analyses of the SIF at the tips of the cracks in terms of superposition of the effects for applied loads and residual stresses are able to explain the experimental outcomes of run-out tests.

Acknowledgements

The activities were carried out in the frame of research contracts between LucchiniRS and Politecnico di Milano (Dept. Mechanical Engineering). The authors acknowledge permission to publish the present results.

References

References

[1] K. Hirakawa, K. Toyama, M. Kubota, The analysis and prevention of failure in railway axles, International journal of fatigue 20 (2) (1998) 135–144.

[2] P. Hutař, P. Pokorný, J. Poduška, R. Fajkoš, L. Náhlík, Effect of residual stresses on the fatigue lifetime of railway axle, Procedia Structural Integrity 4 (2017) 42–47.

[3] S. Wu, Z. Xu, Y. Liu, G. Kang, Z. Zhang, On the residual life assessment of high-speed railway axles due to induction hardening, International Journal of Rail Transportation 6 (4) (2018) 218–232.

[4] W. Maxwell, B. Dudley, A. Cleary, J. Richards, J. Shaw, Measures to counter fatigue failure in railway axles, Proceedings of the Institution of Mechanical Engineers 182 (1) (1967) 89–108.

[5] V. Grubisic, G. Fischer, Procedure for reliable durability validation of train axles, Materialwissenschaft und Werkstofftechnik: Entwicklung, Fertigung, Prüfung, Eigenschaften und Anwendungen technischer Werkstoffe 37 (12) (2006) 973–982.

[6] D. Regazzi, S. Beretta, M. Carboni, An investigation about the influence of deep rolling on fatigue crack growth in railway axles made of a medium strength steel, Engineering Fracture Mechanics 131 (2014) 587–601.

[7] H. Guechichi, L. Castex, J. Frelat, G. Inglebert, Predicting residual stresses due to shot-peening, Impact surface treatment (1986) 11–22.

[8] A. Sackfield, D. Hills, Some useful results in the classical hertz contact problem, The Journal of Strain Analysis for Engineering Design 18 (2) (1983) 101–105.

[9] J.-F. Antoine, C. Visa, C. Sauvey, G. Abba, Approximate analytical model for hertzian elliptical contact problems, Journal of Tribology 128 (3) (2006) 660–664.

[10] D. Regazzi, S. Cantini, S. Cervello, S. Foletti, Optimization of the cold-rolling process to enhance service life of railway axles, Procedia Structural Integrity 7 (2017) 399–406.

[11] B. STANDARD, En 13261 railway applications—wheelsets and bogies—wheelsets—product requirements.

[12] D. Regazzi, S. Cantini, S. Cervello, S. Beretta, S. Foletti, J. Blaha, L. Boronkai, Cold rolling of railway axles – process optimisation and advantages in operation, XIX International wheelset congress june 16-20, 2019 Venice, Italy.

[13] European project euraxles deliverable 3.2: „report on small scale and full scale testing results".

[14] EN13103 - Railway Applications - Wheelsets and Bogies - Non Powered Axles - Design Method (ISO 2001).

[15] S. Cantini, M. Carboni, Ultrasonic inspection of solid railway axles by a phased array rotating probe, XIX International Wheelset Congress, Venice.

[16] M. Carboni, S. Beretta, S. Cantini, D. Regazzi, An analysis of the effect of compressive residual stresses due to roll-forming onto fatigue crack propagation in railway axles, in: 17th International Wheelset Congress, UNIFE e ERWA, 2013, pp. 106–114.

[17] A. Watson, Implications of Impact Damage on the Structural Integrity of Axles, available at http://esistc24.mecc.polimi.it/BERLIN.html (2010).

[18] S. Beretta, M. Carboni, A. L. Conte, D. Regazzi, S. Trasatti, M. Rizzi, Crack growth studies in railway axles under corrosion fatigue: Full-scale experiments and model validation, Procedia Engineering 10 (2011) 3650–3655.

[19] S. Beretta, A. L. Conte, J. Rudlin, D. Panggabean, From atmospheric corrosive attack to crack propagation for a1n railway axles steel under fatigue: damage process and detection, Engineering Failure Analysis 47 (2015) 252–264.

[20] F. Moretti, S. Beretta, A. L. Conte, D. Straub, Corrosion-fatigue under rainwater of a q&t steel: experiments and probabilistic description, Procedia Engineering 74 (2014) 12–17.

[21] S. Wu, C. Li, Y. Luo, H. Zhang, G. Kang, A uniaxial tensile behavior based fatigue crack growth model, International Journal of Fatigue 131 (2020) 105324.

[22] X. Wang, S. Lambert, Local weight functions for semi-elliptical surface cracks in finite thickness plates, Theoretical and Applied Fracture Mechanics 23 (3) (1995) 199 – 208.

[23] W. T. KOITER, General theorems for elastic plastic solids, in: Progress in Solid Mechanics, North Holland Press, 1960, pp. 167–221.

[24] A. Ponter, A general shakedown theorem for elastic/plastic bodies with work hardening.

[25] K. L. Johnson, Contact mechanics, Cambridge university press, 1987.

[26] M. Carboni, D. Regazzi, Effect of the experimental technique onto r dependence of δkth, Procedia Engineering 10 (2011) 2937–2942.

[27] R. Pippan, L. Plöchl, F. Klanner, H. Stüwe, The use of fatigue specimens precracked in compression for measuring threshold values and crack growth, Journal of testing and evaluation 22 (2) (1994) 98–103.

[28] B. Tabernig, R. Pippan, Determination of the length dependence of the threshold for fatigue crack propagation, Engineering Fracture Mechanics 69 (8) (2002) 899–907.

[29] J. Maierhofer, R. Pippan, H.-P. Gänser, Modified nasgro equation for physically short cracks, International Journal of Fatigue 59 (2014) 200–207.

[30] J. Maierhofer, H. Gänser, R. Pippan, Modified kitagawa–takahashi diagram accounting for finite notch depths, International Journal of Fatigue 70 (2015) 503–509.

[31] S. Kolitsch, H.-P. Gänser, J. Maierhofer, R. Pippan, Fatigue crack growth threshold as a design criterion-statistical scatter and load ratio in the kitagawa-

takahashi diagram, in: IOP Conference Series: Materials Science and Engineering, Vol. 119, IOP Publishing, 2016, p. 012015.

[32] S. Beretta, M. Carboni, G. Fiore, A. L. Conte, Corrosion–fatigue of A1N railway axle steel exposed to rainwater, Int. J. Fatigue 32 (2010) 952–961.

[33] S. Beretta, F. Sangalli, J. Syeda, D. Panggabean, J. Rudlin, Raai project: Life-prediction and prognostics for railway axles under corrosion-fatigue damage, Procedia Structural Integrity 4 (2017) 64–70.

[34] U. Zerbst, S. Beretta, G. Köhler, A. Lawton, M. Vormwald, H. T. Beier, C. Klinger, I. Černỳ, J. Rudlin, T. Heckel, et al., Safe life and damage tolerance aspects of railway axles–a review, Engineering Fracture Mechanics 98 (2013) 214–271.